Lab on a Chip

Accepted Manuscript

ROYAL SOCIETY OF CHEMISTRY

www.rsc.org/loc

Spatiotemporal norepinephrine mapping using a high-density CMOS microelectrode array

John B. Wydallis,[a] Rachel M. Feeny,[a] William Wilson,[b] Tucker Kern,[b] Tom Chen,[b] Stuart Tobet,[c] Melissa M. Reynolds,[a] Charles S. Henry[a,d]*

[a] *Department of Chemistry, Colorado State University, Fort Collins, Colorado 80523-1872*

[b] *Department of Electrical and Computer Engineering, Colorado State University, Fort Collins, Colorado 80523-1872*

[c] *Department of Biomedical Sciences, Colorado State University, Fort Collins, Colorado 80523-1872*

[d] *Department of Chemical & Biological Engineering, Colorado State University, Fort Collins, Colorado 80523*

Corresponding Author:
**Phone: 1-970-491-2852. Fax: 1-970-491-1801. E-mail: chuck.henry@colostate.edu*

Abstract

A high-density amperometric electrode array containing 8,192 individually addressable platinum working electrodes with an integrated potentiostat fabricated using Complementary Metal Oxide Semiconductor (CMOS) processes is reported. The array was designed to enable electrochemical imaging of chemical gradients with high spatiotemporal resolution. Electrodes are arranged over a 2 mm × 2 mm surface area into 64 subarrays consisting of 128 individual Pt working electrodes as well as Pt pseudo-reference and auxiliary electrodes. Amperometric measurements of norepinephrine in tissue culture media were used to demonstrate the ability of the array to measure concentration gradients in complex media. Poly(dimethylsiloxane) microfluidics were incorporated to control the chemical concentrations in time and space, and the electrochemical response at each electrode was monitored to generate electrochemical heat maps, demonstrating the array's imaging capabilities. A temporal resolution of 10 ms can be achieved by simultaneously monitoring a single subarray of 128 electrodes. The entire 2 mm × 2 mm area can be electrochemically imaged in 64 seconds by cycling through all subarrays at a rate of 1 Hz per subarray. Monitoring diffusional transport of norepinephrine is used to demonstrate the spatiotemporal resolution capabilities of the system.

Keywords: CMOS, microelectrode array, norepinephrine, spatiotemporal resolution, microfluidics

Introduction

Molecular gradients are important driving forces in biology, directing phenomena such as chemotaxis,[1-3] cancer metastasis,[4] and cell-to-cell communication.[5-7] These processes occur over multiple length scales, ranging from synaptic gaps in angstroms to entire organs in centimeters, and time periods ranging from milliseconds to minutes. The ability to simultaneously monitor chemical gradients and observe cellular responses to those gradients across multiple length scales can provide a critical foundation for understanding biological phenomena.

Monitoring biological processes driven by molecular gradients requires a system capable of generating images with high spatiotemporal resolution and chemical selectivity. Optical and fluorescence microscopies have long been used to observe molecular gradients in biology. Microscopy techniques are ideal in many respects for monitoring chemical gradients in biological systems with spatial and temporal resolution. Unstained living tissue can be imaged using endogenous fluorophores, such as nicotinamide adenine dinucleotide (NADH) and hemoglobin,[8, 9] avoiding the necessity for exogenous probes. Genetic modification, stains, and probes, including fluorescent proteins, quantum dots, and metal chelates can be used to expand the library of molecules detectable by fluorescence techniques, but many species remain inaccessible or have altered activity when conjugated with fluorescent probes.[10-12] Other techniques such as mass spectrometry can detect a large library of molecules with spatial resolution, though these systems typically lack the temporal resolution required to monitor dynamic changes in concentration gradients, as tissues are no longer viable at the time of analysis.[13, 14]

Electrochemistry can provide an alternative way to create a chemical map or “image” that can augment observations from traditional microscopy by detecting, with spatial and temporal resolution, changes in key signaling molecules that cannot be readily measured using microscopy methods. Electrochemical imaging on a microscopic scale has previously been

described in the context of scanning electrochemical microscopy (SECM),[15-17] microfluidic sampling devices,[18, 19] and microelectrode arrays.[20-24] SECM measures current response from a single electrode rastered over a surface to generate images.[15-17] SECM can provide evidence of chemical release with high spatial resolution but requires physical scanning over the surface and thus has limited temporal resolution. Microelectrode arrays offer improved temporal resolution because the electrodes do not move and multiple electrodes can be operated simultaneously. The Baltes, Hierlemann, and Matsue groups have described micro- and nanoelectrode systems fabricated from Complementary Metal Oxide Semiconductor (CMOS) techniques as analytical tools.[25-30] These reports use high-density electrode systems to map cellular electrical signals with subcellular resolution or use redox cycling to generate electrochemical responses to image chemical distributions. While effective, most electrode array-based imaging applications have used tens of electrodes for cellular or sub-cellular imaging or use larger arrays to define voltage gradients across neuronal networks.[20, 21, 31-33] Arrays with higher electrode density and/or large numbers of electrodes have primarily been employed for impedance or voltage-based sensing and not amperometric detection.[23, 34-38] As a preliminary study of the capabilities of an electrode array to image chemical distributions on the scale of an *ex vivo* tissue slice, the system described here was used to image controlled distributions of norepinephrine as a model neurotransmitter.

The system described here uses a high-density electrode array with an on-board potentiostat to make amperometric measurements across a 2 mm x 2 mm array. The array has a spatial resolution of 30 µm, a temporal resolution of 10 ms per 250 µm x 250 µm subarray region, and contains 8,192 individual Pt microelectrodes in addition to on-board reference and auxiliary electrodes. The array was fabricated using standard commercial Complementary Metal Oxide Semiconductor (CMOS) techniques with an added lift-off step to give the final Pt layer for the working electrodes. The die size fits onto the stage of an upright microscope so that optical and electrochemical images can be obtained simultaneously. Images were obtained for

norepinephrine gradients formed *via* either diffusion or hydrodynamic flow directed using a microfluidic device.

Materials and Methods

Materials and instrumentation

All chemicals were at least of ACS grade and used as received without additional purification. SU-8 2075 photoresist was obtained from MicroChem (Westborough, MA). Hexamethyldisilazane (HMDS) and (±)-norepinephrine (+)-bitartrate salt were purchased from Sigma-Aldrich (St. Louis, MO). Sylgard 184 poly(dimethylsiloxane) (PDMS) oligomer and cross-linker were obtained from Dow Corning (Midland, MI). Neurobasal-A media without phenol red was purchased from Life Technologies Corporation (Carlsbad, CA) and was used in all electrochemical experiments to demonstrate compatibility with solutions required for sustaining *in vitro* cell and tissue culture. Dyes (FD&C Red #40 and Blue #1) used for solution visualization were purchased from Kroger (Cincinnati, OH). External power supplies (HP E3630A and E3631A Triple Output DC Power Supplies, Hewlett Packard, Palo Alto, CA) were used to power the system containing the electrode array chip. Optical images and videos were collected using a commercial smartphone (Apple Inc., Cupertino, CA) and a fluorescent magnifier light (LumaPro, W. W. Grainger, Lake Forest, IL). Chip control and data collection were achieved using ADLINK DAQe-2200 data acquisition board. Data post-processing including electrochemical heat map generation was performed using a suite of MATLAB functions (32 bit and 64 bit, Mathworks, Inc., Natick, MA). The electrode array was imaged using a ZeScope optical profilometer (Zygo, Middlefield, CT) and a JSM-6500F scanning electron microscope (JEOL USA Inc., Peabody, MA).

Electrode array design, fabrication, and operation

Chip fabrication and operation. Figure 1 shows optical profilometry and scanning electron microscopy (SEM) images of individual electrodes, a single subarray, and the entire array as well as a photograph of the system after mounting in its ceramic packaging. The electrode array chip was designed in a 0.5-µm 4-layer metal CMOS process. The top layer metal was used for patterning Pt electrodes. The metal layers 1-3 provided necessary routing for the chip. Manufacturing of the electrode array chip was performed by Avago Technologies on 8-inch wafers using Avago's fabrication facility in Fort Collins, Colorado. The die size is 1.9×1.9 cm^2. Extensive details on the microfabrication process are provided in the supplementary section (Supplementary Figures 1 and 2). The on-chip potentiostat has a voltage regulating error of no more than 8 mV in amperometry mode. In voltammetry mode, it is capable of providing up to 10 kV s^{-1} scan rate with the same voltage regulating error. The on-chip control logic also provides flexibility of connecting any electrodes in a subarray directly to the chip I/O pins to allow direct access of electrodes using external potentiostats.

A 96-input data acquisition card (ADLINK DAQe-2200 series) was used, allowing cycling through 96 of the 128 electrodes on each of the 64 subarrays at set intervals to provide imaging results. In the experiments described here, the data were collected from the array by monitoring individual subarrays and cycling through each subarray vertically, starting in the upper-right corner of the array and ending in the bottom-left corner. The subarray switching parameters are definable by the user in custom-designed MATLAB functions through a windows-based graphical user interface. The current response at individual electrodes was converted to color intensity and plotted to generate electrochemical heat maps using a custom MATLAB program. A table of electrical specifications of the microchip can be found in Supplementary Table 1.

Electrode array format. All 8,192 working electrodes are located at the center of the chip in a 2 mm $\times$ 2 mm area. Electrodes were grouped in 64 subarrays each with 128 electrodes. Each subarray has its own Pt pseudo-reference electrode (RE) and counter electrode (CE). The

design of the working electrodes was previously optimized and used for biomarker detection in a microfluidic manifold.[39, 40] Figure 2 shows the arrangement of 128 working electrodes and RE and CE in each subarray. The electrode array chip is housed in a 280-pin ceramic cavity-up PGA package. There are 128 I/O pads on the ceramic PGA package dedicated to the electrodes in subarrays. All 128 electrodes in a given subarray can be selected and connected to the I/O pads through an on-chip 64-to-1 multiplexer. Finally, the electrodes were connected to on-board logic and a potentiostat circuit capable of addressing 128 electrodes in a subarray as well as switching between subarrays. Schematics and further details of the circuit layout and operation are provided in the supplementary section (Supplementary Figures 3-7).[41] For all experiments described here, a 100 Hz data collection rate was used for an active subarray, and subarrays were cycled at a switching rate of 1 Hz when applicable. The on-chip potentiostat was used to apply an oxidation potential of +0.6 V (vs. Pt) for norepinephrine detection and a custom MATLAB script was used to generate electrochemical heat map images and videos for all experiments.

Fabrication of microfluidic devices

Microfluidics were interfaced with the chip using a combination of soft lithography[42, 43] and laser cutting.[44, 45] Wafers and molds were coated with HMDS and baked at 115 ºC for 15 min for easy removal of the PDMS. All microfluidics were fabricated using two layers of PDMS. The bottom layer, which interfaces directly with the CMOS chip, was a 2-mm thick layer of a degassed 30:1 mixture of PDMS oligomer and cross-linker. This PDMS formulation gave higher adhesion to the CMOS chip, allowing for higher flow rates without leakage. After curing the first layer, a 3-mm thick layer of a degassed 10:1 mixture of PDMS oligomer and cross-linker was poured directly on top of the first layer and cured at 80 ºC. This second layer was included to improve the structural integrity of the fluidics and to prevent adhesion to the poly(methylmethacrylate) (PMMA) compression plate described below. Wells used to contain

samples over the electrode array were fabricated by making these two layers on a pristine silicon wafer (Silicon Inc., Boise, ID). A biopsy punch (Robbins Instruments, Inc., Chatham, NJ) was used to create a 10-mm diameter well in the PDMS.

A Y-shaped microfluidic flow channel was fabricated using soft lithography.[42, 43] SU-8 2075 was spin coated onto a 10-cm diameter silicon wafer to achieve a final feature height of 104 ± 1 µm ($n = 7$) as measured by optical profilometry. A Y-shaped microfluidic channel 2.5 mm wide and 7 mm long, with entrance channels 1.75 mm wide and 4.5 mm long was used. PDMS was poured and cured as described above to make the device. A biopsy punch was used to create 1-mm diameter inlets and outlets to interface the device with vinyl PVC tubing (1/32" ID, 3/32" OD, Thermo Fisher Scientific, Waltham, MA), stainless steel connectors (Loctite, Henkel Corporation, Westlake, OH), and NE-1000 Single Syringe Pumps (New Era Pump Systems, Farmingdale, NY) for fluid control.

A second microfluidic device was fabricated to allow fluid transfer across the array *via* head pressure and consisted of two reservoirs connected by a straight channel. Standard photolithography was performed using SU-8 2075 to generate a mold for a microfluidic channel with dimensions 82 µm × 2.5 mm × 6.0 mm. The mold was treated with HMDS, and two layers of PDMS were created as described above. A 5-mm diameter reservoir was punched at both channel ends using a biopsy punch.

A poly(methylmethacrylate) (PMMA) compression manifold was used to prevent fluid leaks from the Y-channel at high flow rates by applying additional pressure to the PDMS on the CMOS chip surface. The plate was cut from 1/8-in thick PMMA (Fort Collins Plastics, CO) using a CO_2 laser engraving system (30 W Epilog, Golden, CO). The plate contained 3-mm diameter holes for access to the inlets and outlet of the channel, a space for the arm of the socket used to interface the silicon chip with the printed circuit board (Textool™ Burn-In Grid ZIP Socket, 3M, Saint Paul, MN), and holes to attach the plate to the printed circuit board. Nylon screws (1.5 in)

and wing nuts were used to hold the plate in place and increase the amount of pressure applied to the PDMS. An image of the setup can be seen in Supplementary Figure 8.

Diffusion of norepinephrine across a subarray

Electrochemical detection of norepinephrine with spatial and temporal resolution was studied using a single subarray (96 of 128 electrodes). A 10-mm diameter well was placed on the CMOS chip with the array positioned in the lower right region of the well and 200 µL of media was added to well. MATLAB was used to monitor a single subarray throughout the entire experiment. A 10-µL drop of 100 mM norepinephrine in media was added to the top left region of the well, resulting in a final norepinephrine concentration of 4.8 mM after complete diffusion. The current resulting from the oxidation of norepinephrine was collected on the subarray as the solution travelled throughout the well.

Norepinephrine diffusion across array

The spatial and temporal resolution of the array was next studied by monitoring slow fluid transport controlled by head pressure and diffusion. Media and a norepinephrine solution were prepared with dye for visualization. Blue media was used as a baseline and red media was used to indicate the presence of norepinephrine in the media. The flow of media containing norepinephrine was controlled by the relative head pressure in each reservoir. First, 20 µL of media was added to one reservoir to fill the flow channel with media and establish a baseline. Next, 19 µL of 10 mM norepinephrine was added to the second reservoir, and additional 0.5-µL aliquots of 10 mM norepinephrine were added to the second reservoir until the head pressure increased enough to begin to push the norepinephrine into the connecting channel. Head pressure and diffusion then slowly drove norepinephrine across the array and the resulting current was monitored across the array.

Bimodal distribution of norepinephrine across the array

Electrochemical images of controlled chemical distributions were generated by using a Y-shaped microfluidic channel on the CMOS chip to produce a bimodal gradient of norepinephrine across the array. Media and a norepinephrine solution were prepared with dyes as described above. Fluid control was achieved using two syringe pumps. Baseline signals were collected by flowing media across the array at 100 µL min^{-1}. The syringe pump containing the 10 mM norepinephrine solution was then started at 50 µL min^{-1} while the media was simultaneously decreased to a flow rate of 50 µL min^{-1} to maintain a total flow rate of 100 µL min^{-1} generating a bimodal norepinephrine gradient across the array.

A similar experiment was carried out to position the bimodal gradient over different portions of the array. After flowing media at 100 µL min^{-1} to establish a baseline, the flow rates were adjusted to have the 10 mM norepinephrine solution sequentially contribute to 25, 50, 75, and 100% of the total 100 µL min^{-1} flow rate, cycling through the entire array at least once between each change in flow rate. Video of the flow was taken using a commercial smartphone to compare to the electrochemical heat maps and is available in the supplementary section.

Results and Discussion

The high-density Pt microelectrode array described here was designed as a platform for imaging chemical distributions with high spatiotemporal resolution. Unlike previous examples of electrode-based imaging arrays, amperometric current was measured (as opposed to impedance) using an on-chip potentiostat. Electrode spacing in a high-density array determines the spatial resolution of the system and on-board electronics control the temporal resolution. Chemical distributions were controlled across the array using simple microfluidics to generate electrochemical images for demonstration of the spatiotemporal capabilities of the array. Variability among electrodes has been observed, and experiments are underway to understand the cause of variation in sensitivity. Slight differences in the electrodes, such as raised edges or small changes in surface area may be resulting in significant differences in signal. The short-

term solution employed here is the use of standards, and a thorough investigation of electrode variability will be performed prior to using this platform for quantitative spatiotemporal imaging of chemical release from live tissue.

Diffusion of norepinephrine across a subarray

A norepinephrine gradient was generated by diffusion across the CMOS array to study the temporal resolution of a single subarray. Current was monitored at 96 electrodes on the subarray (Supplementary Video 1) and was plotted as a function of time for three representative electrodes in different locations on the subarray (Figure 3). Due to the limitation of I/Os on the data acquisition system connected to the host computer, a maximum of 96 channels are available, allowing 96 out of 128 to be monitored at any given time. The next generation of the chip will have the ability to read all 128 electrodes through the expanded I/Os on a new data acquisition system on the host computer, eliminating this limitation. A current increase was observed as norepinephrine reached each electrode, with a 6.5, 5.6, and 4.9 nA increase relative to the baseline current occurring at the first exposed electrode, the electrode in the center of the subarray, and the last exposed electrode, respectively. The sequential decrease in signal across the array was a result of norepinephrine dilution throughout the diffusion process. After the 10-µL drop of 100 mM norepinephrine completely diffused into the media contained in the well, the norepinephrine reached a homogenous concentration of 4.8 mM, and the current of all electrodes equalized at 0.15 ± 0.08 nA (n = 96) greater than the media baseline. With a 10-ms time resolution for sampling, capture of the diffusion process is straightforward. The norepinephrine travelled across the diagonal of the subarray in 12 s, which is faster than pure diffusion (predicted to be 113 s),[46] likely due to advective flow caused by the addition of the norepinephrine solution with a pipette. Monitoring the norepinephrine transport across a 250 µm × 250 µm subarray demonstrates that the spatial resolution of 30 µm, dictated by the electrode spacing, and the 10-ms time resolution, determined by the data collection frequency, allow the system to be used for imaging. Methods utilizing thorough mixing or microfluidic devices are

currently being investigated to provide standardized calibration strategies that are independent of diffusion time or the technique of solution addition *via* pipette.

Norepinephrine diffusion across the array

The spatiotemporal resolution of the full array was studied by monitoring fluid transport controlled by combined head pressure and diffusion. A norepinephrine solution containing dye was used to correlate electrochemical images of norepinephrine with optical images of dye during transport across the array. Representative images can be seen in Figure 4, and the complementary video can be found in Supplementary Video 2. A baseline signal (t = 0 s) was collected for approximately one minute before the norepinephrine reached the array. After 88 s, the difference in head pressure between the reservoirs drove the norepinephrine over approximately the first half of the array, with diffusion generating a concentration gradient observed in both the electrochemical heat map and the optical images. Averaging the signal from all electrodes resulted in 1.3 nA distributed across the array as shown in the electrochemical heat map. After additional fluid transport across the array (t = 220 s), the average signal increased to 5.3 nA with the spatial distribution displayed in the electrochemical heat map. These results demonstrate that the array, which is of suitable size for chemically imaging cells in tissue slices, is capable of achieving high spatiotemporal resolution for the detection of electrochemically active species.

Bimodal distribution of norepinephrine

A bimodal gradient of norepinephrine was generated to electrochemically image a controlled chemical distribution over the electrode array. A Y-shaped microfluidic channel was used to direct 10 mM norepinephrine over approximately half of the array while the remaining portion of the array was exposed to media without norepinephrine. A representative electrochemical heat map and corresponding video frame is shown in Figure 5. A signal gradient was observed across each individual subarray, with the highest signal (44 ± 4 nA) on the left-most column, and lowest signal (23 ± 7 nA) to the right. The current decrease is the

result of analyte depletion from upstream electrodes as the norepinephrine flowed from left to right. This phenomenon was not observed across the array as a whole because the on-chip potentiostat cycled through each subarray at a rate of 1 Hz and the linear flow velocity (6.4 mm s^{-1}) was great enough that the solution was refreshed prior to cycling neighboring horizontal subarrays. The vertical position of the interface between the media and the norepinephrine was observed in the heat map to fluctuate by <250 µm with each column of subarrays. The position changed in the 8 s required to cycle to neighboring subarrays due to imperfect fluid control by the syringe pumps.

Control of the interface position was achieved by adjusting volumetric flow rates on the corresponding syringe pumps to demonstrate the spatiotemporal resolution capabilities of the system. A video of the resulting electrochemical heat map is shown in the Supplementary Video 3 and representative heat maps at each interface position can be seen along the top of Figure 6. For quantitative visualization, the signals were plotted as the average current from all electrodes in a horizontal row of eight subarrays representative of each of four sections of the array, with the error bars representing the standard deviation between the subarrays in the row. Each section of the array consists of two rows of subarrays, with Sections 1-4 ordered sequentially from the top of the array to the bottom. The plotted signals were taken after cycling through all 64 subarrays prior to starting the following cycle. A current increase of 23 ± 6 nA was observed to occur on the sections of the array exposed to norepinephrine and the timing correlated with the video. A bubble can be seen in Section 2 in the heat maps in Figure 6 when norepinephrine fills at least 50% of the channel, which can be correlated with the video shown in Supplementary Video 3. The bubble prevented norepinephrine from reaching the surface of the electrodes, decreasing the average signal (110 nA compared to 120 nA) and resulting in a high standard deviation in signal (5-10% RSD) for the row of subarrays. Bubbles would be problematic when imaging live tissue with this platform, so the design of the microfluidic device will be modified to control bubble formation and provide a method to interface live tissue slices

with the electrode array. Monitoring the controlled distributions of norepinephrine and media in space and time demonstrates the ability of the electrode array to generate electrochemical images of gradients and correlate them to optical images with high spatiotemporal resolution, which could provide the ability to image neurotransmitter release from a tissue slice with cellular resolution, elucidating the effects of molecular gradients on cell-to-cell communication and other biological processes.

Conclusions

High-density electrode arrays containing large numbers of electrodes have primarily been used for impedance or voltage-based sensing with limited utilization of amperometric detection. The system described here was designed to augment traditional microscopy methods, offers an additional tool for imaging chemical distributions in biological systems, and has been used to electrochemically image distributions of norepinephrine standard solutions as a model neurotransmitter. The microelectrode array described is composed of 8,192 platinum working electrodes in a 2 mm × 2 mm area. PDMS microfluidics provided fluid control over the array to image distributions of norepinephrine. The density of the electrode array provided 30-µm spatial resolution, while the on-chip potentiostat and on-board electronics allowed norepinephrine detection with a maximum temporal resolution of 10 ms, as demonstrated by monitoring diffusion of norepinephrine across a single subarray. A larger area of 2 mm × 2 mm could be monitored by switching through subarrays at a rate of 1 Hz. This electrochemical imaging system will be implemented in the future for monitoring chemicals released from live tissue slices with 30 µm spatial resolution. This system has the potential to elucidate the effects of chemical gradients on biological processes such as chemotaxis, cancer metastasis, and directed cell migration.

Acknowledgements

This work is supported in part by National Science Foundation Grant No. GDE-0841259. The silicon-based microelectrode chip was manufactured by Avago Technologies. Their technical assistance and generous support for this project are greatly appreciated.

Figures

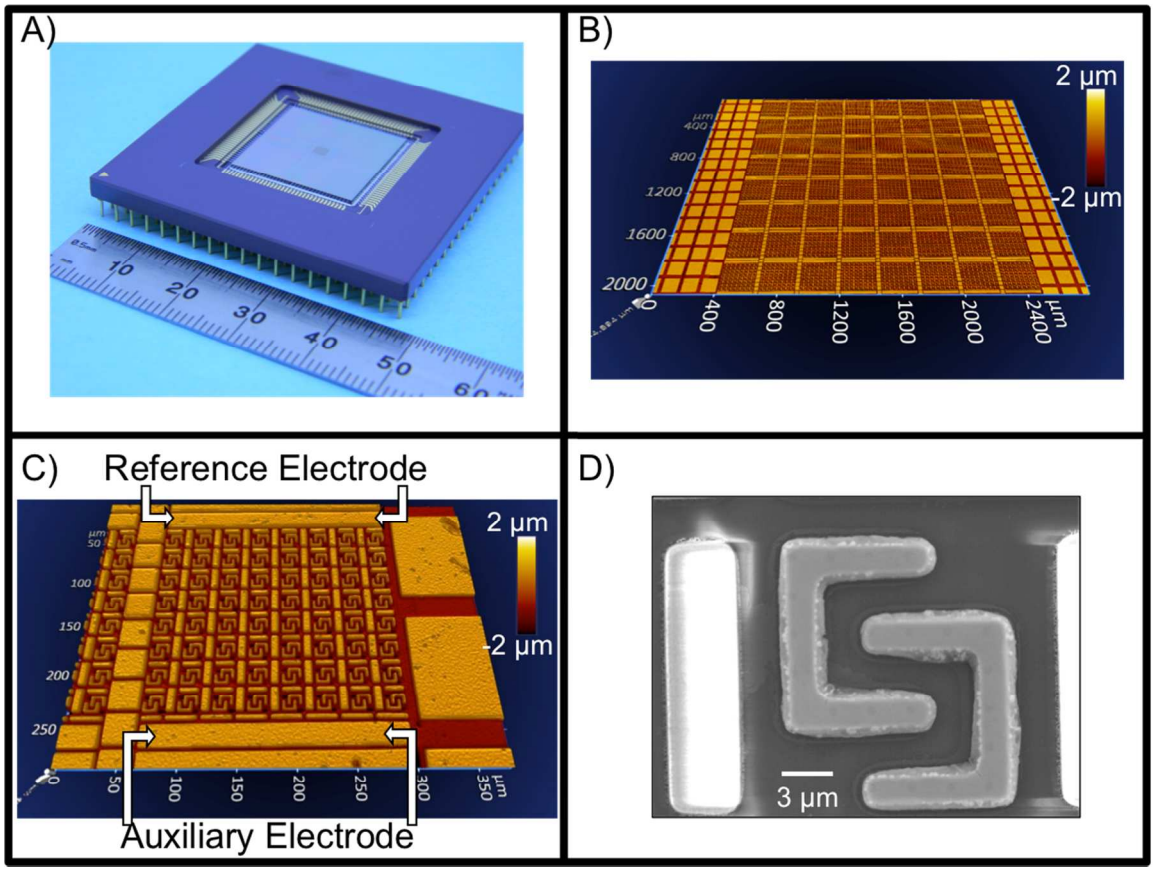

Figure 1. Images of the high-density electrode array. A) Photograph of CMOS chip containing electrodes and on-chip potentiostat. B) Optical profilometry image of entire array showing 64 subarrays. C) Optical profilometry image of a single subarray comprised of 128 working electrodes and shared auxiliary and pseudo-reference electrodes. D) SEM image of two interdigitated platinum working electrodes 12.5 µm long on the y-axis.

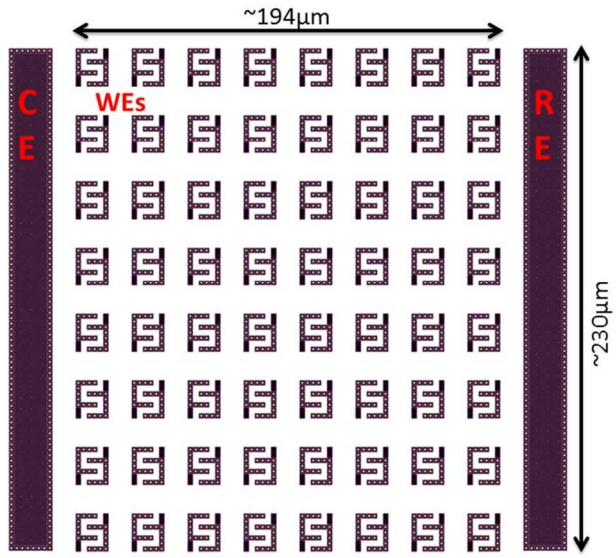

Figure 2. A single subarray of 128 working electrodes, one pseudo-reference electrode, and one auxiliary electrode.

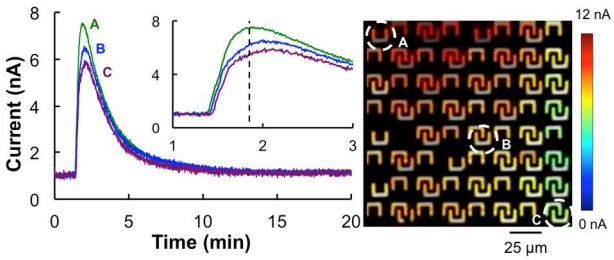

Figure 3. Left) Diffusion of norepinephrine across a subarray. Norepinephrine was added at the top left corner of the subarray. Amperograms correspond to electrodes indicated on the heat map on the right. Electrodes closest to the source of the norepinephrine reach the highest signal, and all electrodes end at the same signal after the norepinephrine has completely diffused. The closest electrodes also detect an increase in signal prior to those located across the subarray. Inset is an expanded view of the peak region showing the difference in both current and timing of the maximum. Right) A still image of the heat map was taken at the time indicated by the vertical dashed line on the inset plot. Supplementary Video 1 shows heat map video. Oxidation potential of +0.6 V (vs. Pt). Data collection rate 100 Hz for all electrodes on subarray.

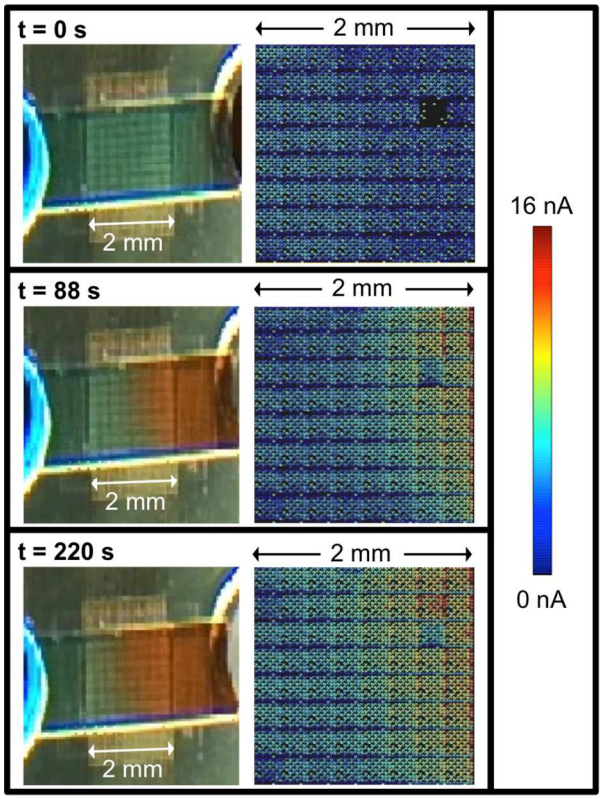

Figure 4. Diffusion of norepinephrine across the array. Optical images and electrochemical heat maps were recorded at the times indicated. Solutions contain dye for visualization. Red solution contains norepinephrine dissolved in neurobasal media, and blue solution is only neurobasal media. Supplementary Video 2 shows corresponding video. Oxidation potential of +0.6 V (vs. Pt). Data collection rate 100 Hz for all electrodes on active subarray. Switching rate between subarrays 1 Hz.

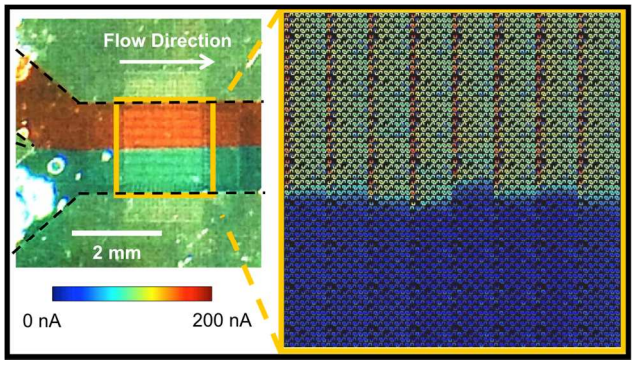

Figure 5. Optical image of bimodal gradient over the 2 mm × 2 mm microelectrode array and corresponding electrochemical heat map. Solutions contain dye for visualization. Red solution contains norepinephrine dissolved in neurobasal media, and blue solution is only neurobasal media. Dashed black lines indicate walls of microfluidic channel. Signal gradient across individual subarrays is due to analyte depletion by upstream electrodes. Oxidation potential of +0.6 V (vs. Pt). Data collection rate 100 Hz for all electrodes on active subarray. Switching rate between subarrays 1 Hz.

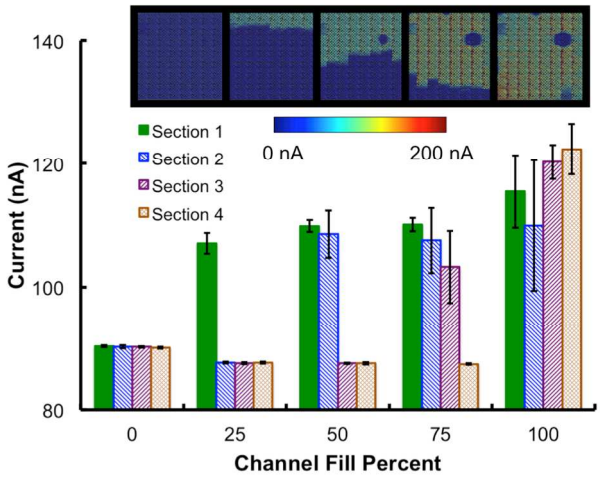

Figure 6. Average signal for each row of subarrays when a bimodal gradient of norepinephrine is generated over different sections of the array. Error bars represent signal standard deviation across the row of subarrays (n = 8). For simplicity, all signals were normalized to the maximum signal detected during the experiment. Heat maps corresponding to the signals plotted are shown to the left. Note that the independent variable is on the y-axis for clarity. In each y-axis category, the position of the data bar corresponds to the row of subarrays analyzed. Supplementary Video 3 shows corresponding video. Oxidation potential of +0.6 V (vs. Pt). Data collection rate 100 Hz for all electrodes on active subarray. Switching rate between subarrays 1 Hz.

References

1. B. J. Kim and M. M. Wu, *Annals of Biomedical Engineering*, 2012, **40**, 1316-1327.
2. R. A. Firtel and C. Y. Chung, *Bioessays*, 2000, **22**, 603-615.
3. W. J. Rosoff, J. S. Urbach, M. A. Esrick, R. G. McAllister, L. J. Richards and G. J. Goodhill, *Nature Neuroscience*, 2004, **7**, 678-682.
4. S. D. Nathanson, *Cancer*, 2003, **98**, 413-423.
5. B. Brucher and I. S. Jamall, *Cellular Physiology and Biochemistry*, 2014, **34**, 213-243.
6. N. C. Guerineau and M. G. Desarmenien, *Cellular and Molecular Neurobiology*, 2010, **30**, 1425-1431.
7. S. C. Ge, S. Koseoglu and C. L. Haynes, *Analytical and Bioanalytical Chemistry*, 2010, **397**, 3281-3304.
8. K. T. Schomacker, J. K. Frisoli, C. C. Compton, T. J. Flotte, J. M. Richter, N. S. Nishioka and T. F. Deutsch, *Lasers in Surgery and Medicine*, 1992, **12**, 63-78.
9. W. R. Zipfel, R. M. Williams, R. Christie, A. Y. Nikitin, B. T. Hyman and W. W. Webb, *Proceedings of the National Academy of Sciences of the United States of America*, 2003, **100**, 7075-7080.
10. Y. Amoh, K. Katsuoka and R. M. Hoffman, *Current Pharmaceutical Design*, 2008, **14**, 3810-3819.
11. C. Kobbert, R. Apps, I. Bechmann, J. L. Lanciego, J. Mey and S. Thanos, *Progress in Neurobiology*, 2000, **62**, 327-351.
12. L. J. Kricka and P. Fortina, *Clinical Chemistry*, 2009, **55**, 670-683.
13. R. M. Caprioli, T. B. Farmer and J. Gile, *Analytical Chemistry*, 1997, **69**, 4751-4760.
14. A. C. Grey, A. K. Gelasco, J. Section, R. A. Moreno-Rodriguez, E. L. Krug and K. L. Schey, *Anatomical Record-Advances in Integrative Anatomy and Evolutionary Biology*, 2010, **293**, 821-828.
15. A. J. Wain, *Electrochemistry Communications*, 2014, **46**, 9-12.
16. S. Amemiya, J. D. Guo, H. Xiong and D. A. Gross, *Analytical and Bioanalytical Chemistry*, 2006, **386**, 458-471.
17. S. Bergner, P. Vatsyayan and F. M. Matysik, *Analytica Chimica Acta*, 2013, **775**, 1-13.
18. A. Selimovic, J. L. Erkal, D. M. Spence and R. S. Martin, *Analyst*, 2014, **139**, 5686-5694.
19. M. M. Mensack, J. B. Wydallis, N. S. Lynn, D. S. Dandy and C. S. Henry, *Lab on a Chip*, 2013, **13**, 208-211.
20. B. N. Kim, A. D. Herbst, S. J. Kim, B. A. Minch and M. Lindau, *Biosensors & Bioelectronics*, 2013, **41**, 736-744.
21. B. Zhang, M. Heien, M. F. Santillo, L. Mellander and A. G. Ewing, *Analytical Chemistry*, 2011, **83**, 571-577.
22. J. Wang, R. Trouillon, J. Dunevall and A. G. Ewing, *Analytical Chemistry*, 2014, **86**, 4515-4520.
23. D. J. Bakkum, U. Frey, M. Radivojevic, T. L. Russell, J. Muller, M. Fiscella, H. Takahashi and A. Hierlemann, *Nature Communications*, 2013, **4**, 12.
24. M. Sen, K. Ino, K. Y. Inoue, T. Arai, T. Nishijo, A. Suda, R. Kunikata, H. Shiku and T. Matsue, *Biosensors & Bioelectronics*, 2013, **48**, 12-18.
25. F. Heer, W. Franks, A. Blau, S. Taschini, C. Ziegler, A. Hierlemann and H. Baltes, *Biosensors & Bioelectronics*, 2004, **20**, 358-366.
26. S. Hafizovic, F. Heer, T. Ugniwenko, U. Frey, A. Blau, C. Ziegler and A. Hierlemann, *Journal of Neuroscience Methods*, 2007, **164**, 93-106.
27. U. Frey, U. Egert, F. Heer, S. Hafizovic and A. Hierlemann, *Biosensors & Bioelectronics*, 2009, **24**, 2191-2198.
28. K. Ino, W. Saito, M. Koide, T. Umemura, H. Shiku and T. Matsue, *Lab on a Chip*, 2011, **11**, 385-388.
29. T. Matsue, *Analytical Sciences*, 2013, **29**, 171-179.

30. J. Rothe, O. Frey, A. Stettler, Y. H. Chen and A. Hierlemann, *Analytical Chemistry*, 2014, **86**, 6425-6432.
31. I. A. Ges, R. L. Brindley, K. P. M. Currie and F. J. Baudenbacher, *Lab on a Chip*, 2013, **13**, 4663-4673.
32. J. Wang, R. Trouillon, Y. Q. Lin, M. I. Svensson and A. G. Ewing, *Analytical Chemistry*, 2013, **85**, 5600-5608.
33. M. K. Zhao, H. Wi, E. J. Lee, E. J. Woo and T. I. Oh, *Physics in Medicine and Biology*, 2014, **59**, 5831-5847.
34. W. Cunningham, K. Mathieson, F. A. McEwan, A. Blue, R. McGeachy, J. A. McLeod, C. Morris-Ellis, V. O'Shea, K. M. Smith, A. Litke and M. Rahman, *Journal of Physics D-Applied Physics*, 2001, **34**, 2804-2809.
35. E. Ferrea, A. Maccione, L. Medrihan, T. Nieus, D. Ghezzi, P. Baldelli, F. Benfenati and L. Berdondini, *Frontiers in Neural Circuits*, 2012, **6**, 14.
36. S. R. I. Gabran, M. T. Salam, J. Dian, Y. El-Hayek, J. L. P. Velazquez, R. Genov, P. L. Carlen, M. M. A. Salama and R. R. Mansour, *Ieee Transactions on Neural Systems and Rehabilitation Engineering*, 2014, **22**, 1072-1082.
37. L. J. Johnson, E. Cohen, D. Ilg, R. Klein, P. Skeath and D. A. Scribner, *Journal of Neuroscience Methods*, 2012, **205**, 223-232.
38. D. Jackel, U. Frey, M. Fiscella, F. Franke and A. Hierlemann, *Journal of Neurophysiology*, 2012, **108**, 334-348.
39. W. Pettine, M. Jibson, T. Chen, S. Tobet, P. Nikkel and C. S. Henry, *Ieee Sensors Journal*, 2012, **12**, 1187-1192.
40. R. M. Feeny, J. B. Wydallis, T. Chen, S. Tobet, M. M. Reynolds and C. S. Henry, *Electroanalysis*, 2014, **26**.
41. M. Duwe, T. Chen and Ieee, Seoul, SOUTH KOREA, 2011.
42. D. C. Duffy, J. C. McDonald, O. J. A. Schueller and G. M. Whitesides, *Analytical Chemistry*, 1998, **70**, 4974-4984.
43. Y. Sameenoi, M. M. Mensack, K. Boonsong, R. Ewing, W. Dungchai, O. Chailapakul, D. M. Cropek and C. S. Henry, *Analyst*, 2011, **136**, 3177-3184.
44. J. P. Davim, C. Oliveira, N. Barricas and M. Conceicao, *International Journal of Advanced Manufacturing Technology*, 2008, **35**, 875-879.
45. I. A. Choudhury and S. Shirley, *Optics and Laser Technology*, 2010, **42**, 503-508.
46. M. Ansari, S. Kazemi, M. A. Khalilzadeh, H. Karimi-Maleh and M. B. P. Zanousi, *International Journal of Electrochemical Science*, 2013, **8**, 1938-1948.